

Article

Merkel Cell Polyomavirus Large T Antigen Induces Cellular Senescence for Host Growth Arrest and Viral Genome Persistence through Its Unique Domain

Alexander M. Pham ¹, Luz E. Ortiz ¹, Aron E. Lukacher ¹ and Hyun Jin Kwun ^{1,2,*}

¹ Department of Microbiology and Immunology, Pennsylvania State University College of Medicine, Hershey, PA 17033, USA

² Penn State Cancer Institute, Hershey, PA 17033, USA

* Correspondence: hxk479@psu.edu; Tel.: +1-(717)-531-7241

Abstract: Senescent cells accumulate in the host during the aging process and are associated with age-related pathogenesis, including cancer. Although persistent senescence seems to contribute to many aspects of cellular pathways and homeostasis, the role of senescence in virus-induced human cancer is not well understood. Merkel cell carcinoma (MCC) is an aggressive skin cancer induced by a life-long human infection of Merkel cell polyomavirus (MCPyV). Here, we show that MCPyV large T (LT) antigen expression in human skin fibroblasts causes a novel nucleolar stress response, followed by p21-dependent senescence and senescence-associated secretory phenotypes (SASPs), which are required for MCPyV genome maintenance. Senolytic and navitoclax treatments result in decreased senescence and MCPyV genome levels, suggesting a potential therapeutic for MCC prevention. Our results uncover the mechanism of a host stress response regulating human polyomavirus genome maintenance in viral persistency, which may lead to targeted intervention for MCC.

Keywords: senescence; nucleolar stress response; Merkel cell polyomavirus; large T; p53; p21WAF1; Merkel cell carcinoma; genome maintenance; senolytic



Citation: Pham, A.M.; Ortiz, L.E.; Lukacher, A.E.; Kwun, H.J. Merkel Cell Polyomavirus Large T Antigen Induces Cellular Senescence for Host Growth Arrest and Viral Genome Persistence through Its Unique Domain. *Cells* **2023**, *12*, 380. <https://doi.org/10.3390/cells12030380>

Academic Editors: Isabella Saggio and Romina Burla

Received: 28 November 2022

Revised: 13 January 2023

Accepted: 17 January 2023

Published: 20 January 2023



Copyright: © 2023 by the authors. Licensee MDPI, Basel, Switzerland. This article is an open access article distributed under the terms and conditions of the Creative Commons Attribution (CC BY) license (<https://creativecommons.org/licenses/by/4.0/>).

1. Introduction

Senescence refers to stable cell cycle arrest thought to be an antiproliferative cellular defense mechanism against cancer [1] and viral replication [2]. This process can be induced through a variety of cellular stress responses, such as the DNA damage response (DDR), the nucleolar stress response (NSR), and replicative stresses [1,3], leading to p53 activation and the subsequent upregulation of p21. p21 can induce sustained G1 cell cycle arrest and senescence, thereby preventing cell cycle progression and proliferation [1]. Senescent cells have an altered phenotype compared to their non-senescent counterparts, including the induction of senescence-associated secretory phenotype (SASP) genes, upregulation of anti-apoptotic genes [4], and downregulation of various antiviral signaling pathways [5,6].

Several studies have shown that viral infections can induce cellular senescence as part of the antiviral response [2,7]. Vesicular stomatitis virus titers were reduced when permissive cells were driven into senescence by bleomycin treatment [2]. The infection of fibroblast cells with measles virus induced cell fusion and cellular senescence, indicating the potential of senescence to limit viral replication [8]. On the other hand, there is growing evidence of viruses using senescent cells to their advantage. The replication efficiency of influenza virus and varicella zoster virus (VZV) was higher in senescent cells compared to non-senescent cells [6]. Senescent cells have also been shown to upregulate the entry receptor for dengue virus and severe acute respiratory syndrome coronavirus 2 (SARS-CoV2), yielding enhanced viral entry and infection [9,10]. Because senescent cells are more resistant to apoptosis and have reduced antiviral signaling, this cellular environment could be conducive for persistent viral infections.

These senescent phenotypes could be exploited by MCPyV, a double-stranded DNA tumor virus that causes a persistent infection. MCPyV is a ubiquitous pathogen that can cause Merkel cell carcinoma (MCC), a rare but aggressive skin cancer that mainly affects immunocompromised patients [11]. The MCPyV large tumor antigen (LT) is required for viral genome replication [12] and the restriction of cell proliferation [13,14]. This protein is unique from LT antigens of other human polyomaviruses in that it contains a disordered MCPyV unique region (MUR) domain [15,16]. The MUR domain aids in establishing viral latency through ubiquitination by host E3 ubiquitin ligases [15,17–19] that destabilize MCPyV LT and result in the inhibition of MCPyV DNA replication. Recently, MCPyV replication has been shown to activate host cell senescence, potentially by a variety of intrinsic and extrinsic stresses, although its exact mechanism remains unknown [20]. Here, we investigate the mechanism of MCPyV LT-induced senescence and the role of the MCPyV LT unique domain in a host cellular stress response during human polyomavirus infection, which may explain a critical interplay between the host and a viral pathogen leading to cancer.

2. Results

2.1. MCPyV LT Mediates Cellular Senescence in Human Fibroblast Cells through Its Unique Domain

During our study of MCPyV LT-mediated cell growth regulation [15], we observed significant structural alterations in normal human fibroblasts BJ-hTERT expressing MCPyV LT, including enlarged nuclei and flattened morphology, which are features associated with cellular senescence. Because enlarged nuclei in MCC cases correlate with MCPyV positivity [21], we explored the possibility that senescence, mediated by MCPyV LT, is an integral part of the MCPyV life cycle. To determine if MCPyV LT expression alone induces cellular senescence, we created lentiviruses that encode either MCPyV LT or SV40 LT fused with 2A self-cleaving peptides (P2As) and enhanced green fluorescent proteins (eGFPs) [15] to transduce BJ-hTERT cells; an eGFP-P2A empty vector lentivirus served as a negative control (Figure 1A). Because the MUR domain is unique to MCPyV and regulates cell proliferation [15], we asked if this domain had a role in regulating cell morphological changes and, therefore, senescence. To understand the effect of the MUR domain on MCPyV LT-induced morphological changes, a MCPyV LT mutant with a deletion of the MUR domain (MCPyV LT dMUR) [15] and a SV40 LT with the insertion of the MCPyV LT MUR domain (SV40LT+MUR) [15] were also examined. Only the MCPyV LT-expressing cells strongly stained positive for senescence-associated beta-galactosidase (SA- β -gal), the most common senescent marker, at 14 days post-transduction. Fourteen days post-transduction was chosen as we observed the most morphological changes at this timepoint. SA- β -gal staining was determined by both brightfield microscopic (Figure 1B) and flow cytometric analyses (Figure 1C). Approximately 50% of MCPyV LT-expressing cells were senescent, whereas only 5% or less of cells were senescent for the remaining LT constructs or empty vector. SA- β -gal-positive cells expressing MCPyV LT had a significant increase in nuclear area, approximately twice the size ($>500 \mu\text{m}^2$) of the empty vector and other LT constructs ($225\text{--}250 \mu\text{m}^2$) (Figure 1D). Minimal staining or morphological changes were observed in cells expressing the empty vector, SV40 LT, and SV40LT+MUR. MCPyV LTdMUR expression greatly reduced SA- β -gal staining and nuclear size, indicating the potential of the MUR domain to promote senescence only in the context of MCPyV LT. Notably, the insertion of the MUR domain into SV40 LT did not promote senescence, suggesting that the MUR domain does not directly stimulate senescence and other factors are likely involved in inducing this phenotype. Analyses of mRNAs for a variety of senescence-associated secretory phenotype (SASPs), in which transcripts for *ANKRD1*, *CSF2*, *CXCL1*, *CXCL2*, *EDN1*, *IL-6*, and *IL-8* were markedly upregulated by MCPyV LT expression and only modestly upregulated in MCPyV LTdMUR-expressing cells compared to the eGFP control (Figure 1E), concluded that the MUR domain is required for the induction of senescence.

Senescence is commonly regulated through the activation of the p53/p21 pathway and is often characterized by prolonged G1 cell cycle arrest [1]. Immunoblot analyses revealed that only MCPyV LT led to p21 upregulation (Figure 1F). MCPyV LT-positive cells also showed a substantial upregulation of cyclin E, a G1 phase marker [22–25], indicating G1 cell cycle arrest in a subset of the cell population. In addition, histone H3 phosphorylation at Ser10 (pHH3), a mitotic marker [26], is weakly expressed in the G2 phase [27], and MCPyV LT-positive cells displayed histone H3 phosphorylation at low levels, signifying G2 cell growth arrest [28,29]. In contrast, the MCPyV LTdMUR and SV40 LT+MUR mutants showed no significant p21 or cyclin E upregulation or pHH3 downregulation compared to the eGFP⁺ control cells, implying that growth arrest was specific to wild-type MCPyV LT. Immunofluorescent analyses confirmed that enlarged MCPyV LT senescent cells exhibited high p21 expression (Figure S1A) and lacked pHH3 expression (Figure S1B). These results suggest that only MCPyV LT could activate p21, specifically requiring the MUR domain to induce growth arrest and cellular senescence.

Because Siebels et al. reported that MCPyV replication could induce cellular senescence in primary normal human dermal fibroblast (nHDF) cells [20], we also examined the ability of MCPyV LT to induce senescence in other normal human fibroblast cell lines, including, HFF-1, BJ, and neonatal nHDF cells. At 7 days post-transduction, an enlarged nuclear size (~400 μm^2) was observed in HFF-1 and BJ cell lines by MCPyV LT expression (Figure S2A). Unexpectedly, a nonspecific background staining of SA- β -gal was detected in these cells (Figure S2B). Additionally, senescent phenotypes, including a significantly enlarged nuclear size (>500 μm^2) (Figure S3A) and a drastic upregulation of p21 expression (Figure S3B) were induced by MCPyV LT expression at 7- and 10-days post-transduction in neonatal nHDF cells, although high levels of basal SA- β -gal activity were also observed (Figure S3C). Due to the detection of the high nonspecific SA- β -gal staining pattern in these human fibroblast cell lines, we chose to continue utilizing BJ-hTERT cells to most accurately determine the senescent phenotypes induced by MCPyV LT. These results demonstrate that MCPyV LT expression alone can promote cellular senescence in human fibroblast cell lines.

2.2. MCPyV LT-Mediated Senescence Is DDR-Independent

Senescent growth arrest is often triggered by a persistent DNA damage response [4]. A previous study has shown that MCPyV LT can induce double-stranded breaks and activate the host cell's DDR through p53 activation [13]. To determine whether MCPyV LT induces DDR-dependent senescence, we looked for the presence of gamma-H2AX (γ -H2AX), a biomarker for DNA double-strand breaks [30]. A subset of MCPyV LT-expressing senescent cells with enlarged nuclei (>500 μm^2) were positive for γ -H2AX staining, although some senescent cells were also negative for γ -H2AX staining despite morphologic changes (Figure 2A). Moreover, MCPyV LT-expressing cells with a normal nuclear size (~200 μm^2) were still able to induce a DDR response. Although eGFP, MCPyV LTdMUR, SV40 LT, and SV40 LT+MUR-expressing cells were significantly lower for SA- β -gal staining (Figure 1B,C), 20–30% of cells were positive for γ -H2AX foci formation regardless of the stimulus (Figure S4). These results indicate that wild-type MCPyV LT likely mediates cellular senescence through a DDR-independent manner.

The nucleolar stress response is another mechanism that can induce senescence through p53 activation [31]. This response involves the translocation and reorganization of nucleolar proteins, such as nucleophosmin 1 (NPM1) [32,33], into the nucleoplasm or to the periphery of the nucleolus respectively, subsequently activating the p53/p21 pathway and inhibiting ribosomal biogenesis [32]. Senescent MCPyV LT-expressing cells displayed a distinct ring-like nucleolar NPM1 distribution that can be triggered in response to nucleolar stress (Figure 2B) [33–35]. In contrast, empty vector, MCPyV LTdMUR-expressing cells exhibited a normal speckled NPM1 staining pattern typically found in unstressed cells. Approximately 80% of MCPyV LT-positive cells formed NPM1 nucleolar rings (Figure 2C) and had an enlarged nuclear size (>500 μm^2) (Figure 2D), comparable to the nuclear size of

senescent cells seen in Figure 1C. These results show that MCPyV LT induces a nucleolar stress response.

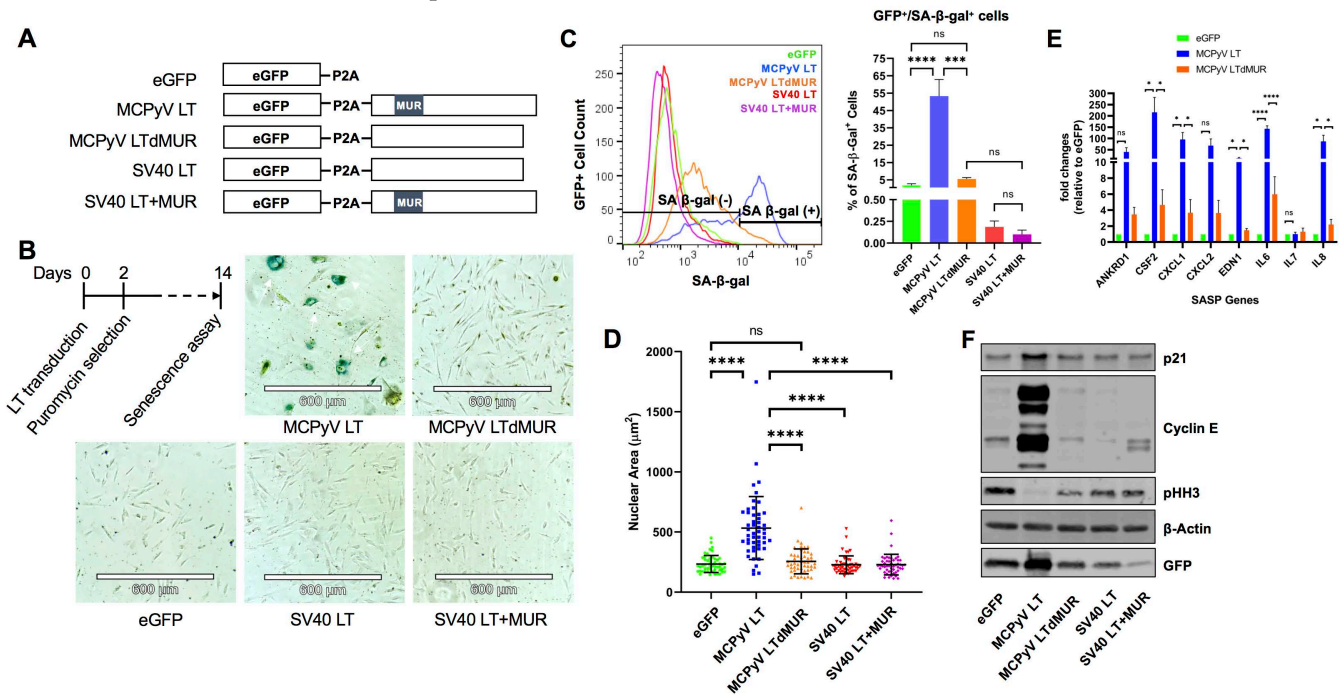


Figure 1. MCPyV LT induces cellular senescence. (A) Lentiviral constructs for LT expression. (B) Senescence assay. Normal BJ–hTERT human fibroblast cells were transduced with either eGFP empty vector or LT constructs and were selected with puromycin at two days post–transduction. A colorimetric senescence-associated β –galactosidase assay (SA– β –gal) was conducted 14 days post–transduction. MCPyV LT–expressing cells with blue staining were positive for SA– β –gal, indicated by white arrows. Images are representative of 3 experiments. (C) Fluorescent intensity of SA– β –gal activity (SA– β –gal⁺) was measured in GFP⁺ (LT–expressing) cells by flow cytometry. MCPyV LT expression significantly increased the number of senescent cells. One–way ANOVA test was used to determine statistical significance (** $p < 0.001$, **** $p < 0.0001$, ns = not significant). Standard error bars represent standard error value, $n = 3$. (D) MCPyV LT promotes senescent phenotypes. Nuclear area (μm^2) of empty vector or LT–transduced BJ–hTERT cells. One–way ANOVA test (**** $p < 0.0001$, ns = not significant). Standard error bars represent mean value with standard deviation, $n = 50$ cells per construct. (E) SASP activation by MCPyV LT. Quantitative reverse transcription polymerase chain reaction (RT–qPCR) analysis of SASP cytokines. Abbreviations—*ANKRD1*: Ankyrin repeat domain 1; *CSF2*: Colony-stimulating factor 2; *CXCL*: chemokine (C–X–C motif) ligand; *EDN1*: Endothelin 1; *IL*: Interleukin. SASPs mRNA levels were substantially upregulated by LT expression except *IL–7*. One–way ANOVA test was used to determine statistical significance (**** $p < 0.0001$, * $p < 0.05$, ns = not significant). Standard error bars represent standard error value, $n = 3$. (F) MCPyV LT activates p21. Growth arrest genes were upregulated in MCPyV LT–expressing cells. Immunoblot of cell cycle–related genes in BJ–hTERT cells transduced with empty vector or LT constructs. β –Actin was used as a loading control.

Phosphorylation of p53 at serine 15 (S15), an upstream event prior to p21 upregulation, can be induced by the NSR [31]. S15 phosphorylation of p53 was noted in MCPyV LT–positive cells marked by the staining of numerous foci in the nucleus, but it was substantially reduced in MCPyV LTdMUR (Figure 2E). SV40 LT constructs exemplified phospho-p53 staining (Figure 2E), but did not induce p21 expression, as shown in Figures 1F and S1A as previously reported in BJ–hTERT and U2OS cells [13,36]. Taken together, these results indicate that MCPyV LT-mediated senescence is associated with the NSR, leading to the activation of the p53/p21 pathway.

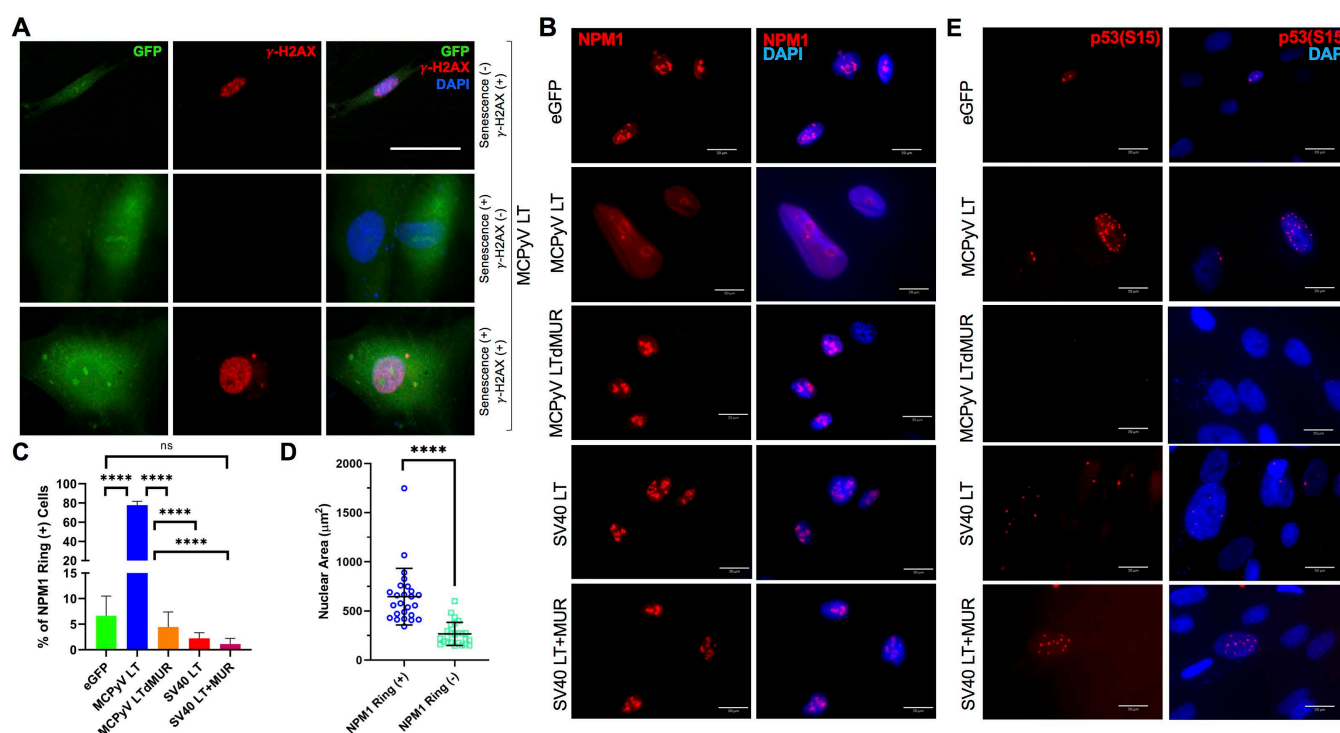


Figure 2. MCPyV LT induces a nucleolar stress response (NSR). **(A)** MCPyV LT–induced senescence is DDR-independent. Immunofluorescent staining for γ -H2AX, a DNA damage marker, in senescent (GFP⁺, nuclear size > 500 μm^2) and non-senescent (GFP⁺, nuclear size = \sim 200 μm^2) MCPyV LT–positive BJ–hTERT cells. Scale bar = 60 μm . **(B)** MCPyV LT reorganizes the nucleolus. MCPyV LT induced a ring–like perinucleolar distribution of NPM1 within the nucleolus, a characteristic of canonical NSR. Immunofluorescent analysis of NPM1 is shown (red). Scale bars = 20 μm . **(C)** MCPyV LT uniquely alters NPM1 structure. The percentage of NPM1 nucleolar ring–positive cells for the empty vector and each LT construct was recorded. Statistical significance was determined using the one–way ANOVA test (**** $p < 0.0001$, ns = not significant). Standard error bars represent mean value with standard error, $n = 30$ cells with 3 replicates. **(D)** Cells with NPM1 reorganization induced by MCPyV LT display senescent phenotypes. Nuclear size (μm^2) of MCPyV LT–expressing cells with or without NPM1 nucleolar rings. Unpaired Student’s t -test (**** $p < 0.0001$, ns = not significant). Standard error bars represent mean value with standard deviation, $n = 25$ cells per condition with 3 replicates. **(E)** MCPyV LT expression triggers the NSR and induces p53 phosphorylation through the MUR. Phospho–p53 (S15) is detected in MCPyV LT–expressing cells.

2.3. MCPyV LT-Induced Senescence Is p21-Dependent

Because p21 has a key role in cellular senescence, we hypothesized that the loss of p21 expression would block MCPyV LT-induced senescence. To determine whether the MCPyV LT-mediated modulation of p53/p21 is required for the onset of senescence, a knockdown of p21 was performed by short hairpin RNA (shRNA) transduction in BJ–hTERT cells expressing MCPyV LT using two shRNA lentiviral constructs, shp21.1 and shp21.2. Transduction with scrambled shRNA (Scr) was used as a control. The knockdown of p21 was confirmed at the mRNA and protein levels in MCPyV LT-expressing cells by RT–qPCR (Figure 3A) and immunoblotting (Figure 3B), respectively. Knockdown using shp21.1 drastically decreased p21 mRNA (\sim 95%) and protein (\sim 75%) levels, while knockdown with shp21.2 reduced p21 mRNA expression to a lesser degree (\sim 40%) and did not decrease p21 protein levels. Dual knockdown with shp21.1 and shp21.2 (shp21.1/2) reduced p21 to similar levels to knockdown with shp21.1 alone. Because it was the most efficient at knocking down p21, the shp21.1 construct (p21KD) was used for the remaining experiments (Figures 4–6). Knockdown of p21 after lentiviral transduction of MCPyV LT reversed cell

cycle arrest, as shown by decreased cyclin E and increased pHH3 expression (Figure 3B). Moreover, p21 knockdown cells no longer exhibited an enlarged and flattened morphology compared to the MCPyV LT-expressing cells transduced with the scrambled shRNA control (Figure 3C). The nuclear area of MCPyV LT-expressing cells was significantly reduced from ~580 μm^2 to ~190 μm^2 , approximately the nuclear size of the eGFP control cells (Figure 3D). SA- β -gal staining confirmed that p21 knockdown largely inhibited MCPyV LT-mediated senescence (Figures 3E and S5) and NSR (Figure 3F), concluding that MCPyV LT-induced senescence is p21-dependent.

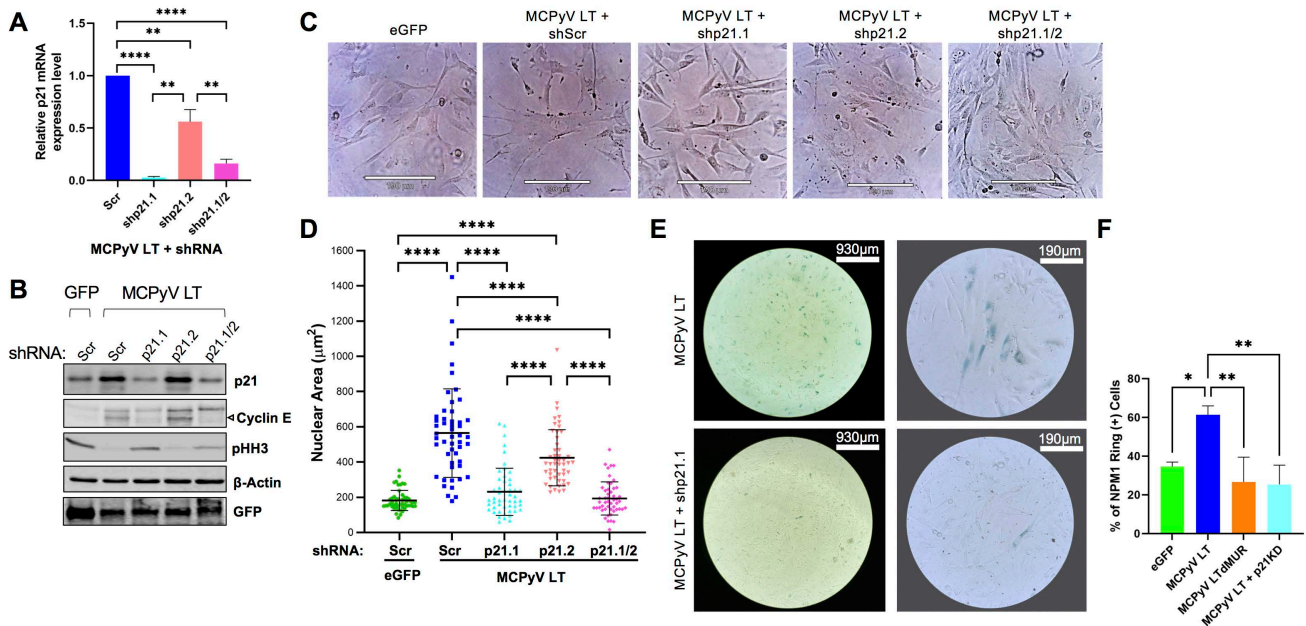


Figure 3. MCPyV LT induces p21-dependent cellular senescence. (A) p21 mRNA levels determined after p21 knockdown in MCPyV LT-positive cells by RT-qPCR. BJ-hTERT cells were transduced with either empty vector or MCPyV LT and selected with puromycin. At 14 days post-transduction, MCPyV LT-expressing cells were transduced with either scrambled (Scr) shRNA or shp21.1, shp21.2, or both (shp21.1/2) for p21 knockdown, and then analyzed seven days later (Day 21). Statistical significance was determined using the one-way ANOVA test (** $p < 0.01$, **** $p < 0.0001$). Standard error bars represent mean value with standard error, $n = 3$. (B) Analysis of p21 knockdown efficiency by immunoblotting. Both p21 and cyclin E protein levels activated in MCPyV LT-expressing cells were reduced by shRNA transduction. The arrow indicates that the major ~50 kDa band of cyclin E. Histone H3 phosphorylation at Ser10 (pHH3), a mitotic marker, is downregulated in MCPyV LT-positive cells with p21 activation, signifying cell cycle arrest. β -Actin was used as a loading control. (C) Senescent morphological changes in MCPyV LT-expressing cells are reversed after p21 knockdown. Brightfield images of empty vector or LT-expressing cells are shown after knockdown. Scale Bar = 190 μm . (D) Abnormal nuclear size change in MCPyV LT-expressing cells is reversed after p21 knockdown. Statistical significance was determined using the one-way ANOVA test (**** $p < 0.0001$). Standard error bars represent mean value with standard deviation, $n = 50$ cells. (E) p21 knockdown reverses senescence. SA- β -gal senescence assay in MCPyV LT-expressing cells was performed after p21 knockdown. (F) p21 knockdown in LT-expressing cells decreased LT-induced NPM1 ring formation. Statistical significance was determined using the one-way ANOVA test (* $p < 0.05$, ** $p < 0.01$). Standard error bars represent mean value with standard error, $n = 25$ cells with 3 replicates.

2.4. Senescent MCPyV LT-Expressing Cells Are Arrested in G2 Phase

p21-induced senescence commonly leads to G1 cell cycle arrest [1]. To verify the cell cycle status and further characterize the growth arrest modulated by MCPyV LT, cell cycle and cell proliferation analyses were performed. Flow cytometric analysis showed that MCPyV LT induced G2 cell cycle arrest, as seen by the enrichment of cells in the G2 phase

(Figures 4A and S6) as previously reported [13,20]. Further analysis of MCPyV LT G1- and G2-arrested cells revealed that these cells were larger than the control and MCPyV LTdMUR-expressing cells, suggesting that these growth-arrested cells were likely senescent (Figure 4B). G2-arrested cells were larger than their G1-arrested counterparts, implying that G2-arrested cells were senescent. This possibility was confirmed by the observation that approximately 70% of MCPyV LT G2-arrested cells were positive for SA- β -gal. In contrast, only ~20% of MCPyV LTdMUR G2 cells were positive for SA- β -gal (Figure 4C). As expected, the knockdown of p21 in MCPyV LT-expressing cells induced cell cycle re-entry (Figure 4A), reduced cell size to eGFP control levels (Figure 4B), and decreased SA- β -gal expression to near MCPyV LTdMUR levels (Figure 4C).

MCPyV LT expression has been shown to reduce cell proliferation through either the C-terminus or the MUR domain [13–15]. To identify if cellular senescence was a potential cause of growth inhibition through the MUR domain, a HoloMonitor (PHI Lab), a non-invasive live-cell imager and counter was utilized [37]. MCPyV LT-expressing cells proliferated slower than their MCPyV LTdMUR counterparts (Figure 4D). Additionally, the incorporation of 5-ethynyl-2'-deoxyuridine (EdU) by MCPyV LT-expressing cells was markedly reduced compared to the MCPyV LTdMUR mutant (Figures 4E and S7). Knockdown of p21 in MCPyV LT-expressing cells reversed growth inhibition induced by MCPyV LT expression (Figure 4D,E). Although p21-dependent senescence often leads to G1 cell cycle arrest [1], our results indicate that MCPyV LT-mediated p21 activation mainly facilitated G2-arrested cellular senescence, negatively regulating cell growth.

2.5. MCPyV LT-Induced Senescence Alters Host Gene Expression Profile

Senescent cells are characterized by the enhanced secretion of cytokines known as SASPs [1]. To further characterize MCPyV LT-induced senescence, RNA sequencing was performed (Figure 5). Multidimensional analyses indicated that replicates were transcriptionally similar and clustered together (Figure S8A). Of note, cells expressing eGFP or dMUR had similar transcriptomes, further demonstrating the importance of the MUR domain on LT function (Figure S8A,B). Additionally, p21 knockdown drastically altered gene expression. Volcano plots illustrated many differentially expressed genes between MCPyV LT- and LTdMUR-expressing cells and in MCPyV LT-expressing cells with p21KD (Figure S8C). A heatmap containing the top 100 differentially expressed genes (DEGs) was generated, comparing eGFP, MCPyV LT, MCPyV LTdMUR, and MCPyV LT+p21KD (Figure 5A, Supplementary Dataset S1). Numerous SASPs, including *CXCL1*, *CXCL2*, *CXCL5*, *IL-1a*, *IL-1b*, *IL-6*, *IL-8*, *SAA1*, and *SAA2*, were identified on this heatmap and MCPyV LT led to a modest upregulation of some of these SASPs compared to the MCPyV LTdMUR and eGFP control. Unexpectedly, p21KD led to a dramatic increase in the expression of inflammatory cytokines, potentially due to cell death induced by p21KD after lentiviral transduction.

To further investigate the changes in gene expression due to MCPyV LT, the MUR domain, and p21-dependent senescence, we generated heatmaps of the top 50 differentially expressed genes (DEGs), comparing MCPyV LT to eGFP, LTdMUR, and p21KD, respectively (Figure 5B, Supplementary Dataset S1). SASPs and senescence genes commonly found as a top DEG were examined. Log₂ fold change of genes and their corresponding *p* values compared to eGFP were plotted (Figure 5C). Cyclin E transcripts were significantly upregulated compared to the empty vector and the dMUR mutant (*p* value < 0.05). Significant SASPs that were upregulated in MCPyV LT-expressing cells compared to eGFP and dMUR mutant cells included *SAA1*, *SAA2*, *CXCL1*, and *CXCL5*. Pathway analyses indicated that MCPyV LT-expressing cells were enriched in senescence-related pathways and downregulated in rRNA and ribosomal metabolic pathways compared to p21KD cells (Figure 5D), reinforcing the conclusion that MCPyV LT promotes the NSR and activates p21-mediated senescence [38]. Genes found in the enriched senescent pathways included numerous histone variants (Supplementary Dataset S1), which have been previously associated with senescence [39]. Some of the expressed aging/senescence-related genes found

highly upregulated in MCPyV LT⁺ cells (*SULF2* [40], namely *MEAP5* [41], *KISS1* [42], and *APOE* [43,44]) were inversely regulated by p21KD (Figure 5C,D).

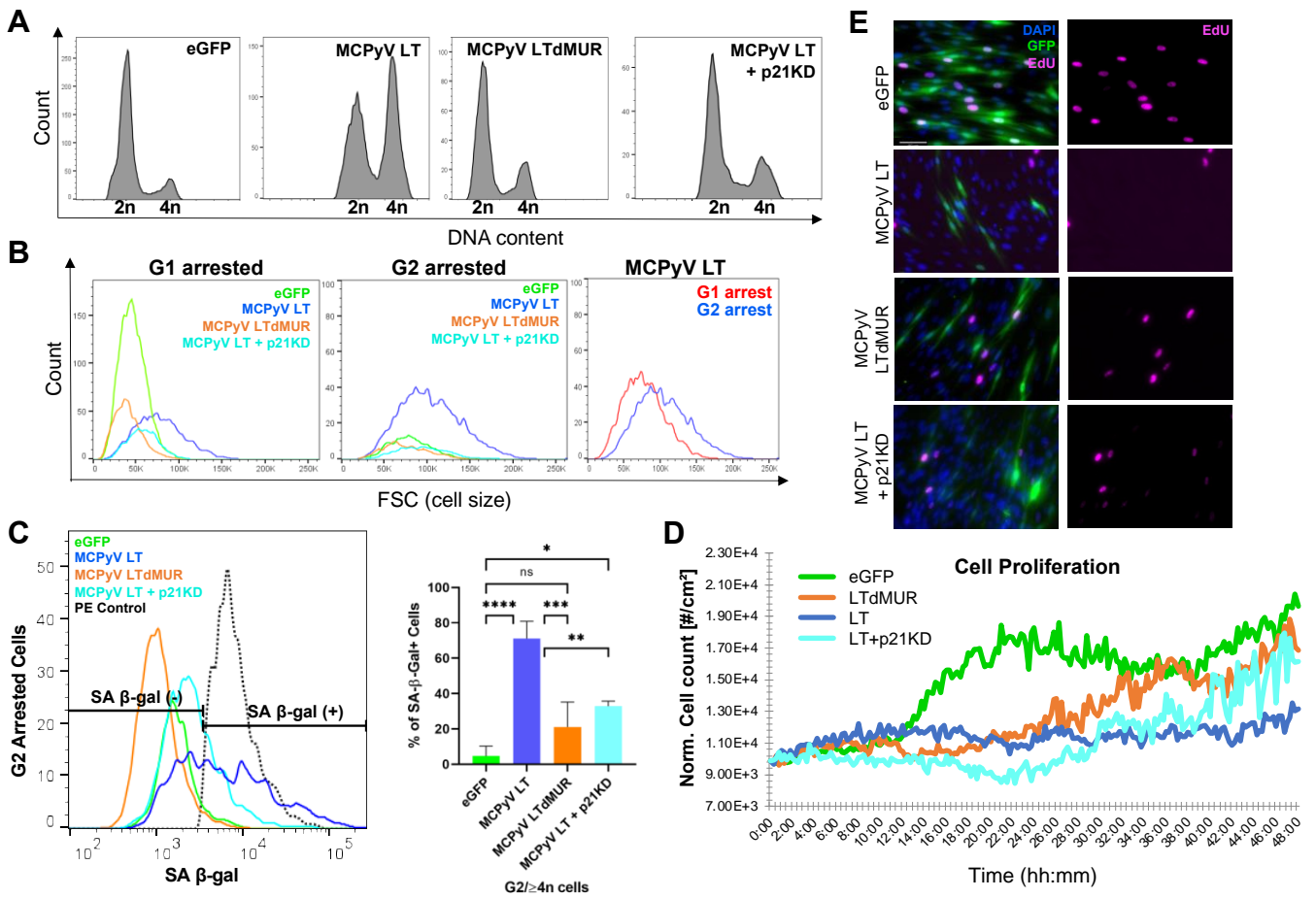


Figure 4. MCPyV LT leads to prolonged G2 cell cycle arrest. (A) MCPyV LT–expressing cells accumulate mainly in G2 phase. Cell cycle analysis of eGFP empty vector, MCPyV LT, MCPyV LTdMUR, and MCPyV LT + p21KD (*shp21.1*) using flow cytometry. Hoechst 33342 was used to stain DNA. A total of 10,000 events were analyzed for each sample, $n = 3$. (B) Histogram of forward scatter (FSC) comparisons of G1– and G2–arrested cells. G1 and G2 cells in MCPyV LT–expressing (GFP⁺) cells were gated and analyzed for cell size using forward scatter (FSC) parameter. Cellular size of G2–arrested cells in MCPyV LT–expressing cells is larger than G1–arrested cells. (C) MCPyV LT–induced senescent cells are arrested mainly in G2. Histogram of SA–β–gal staining (PE) on G2–arrested cells (left). Quantification of G2–arrested/SA–β–Gal⁺ cells by flow cytometry (right). Black dashed line represents PE positive control. Statistical significance was determined using the one–way ANOVA test (* $p < 0.05$, ** $p < 0.01$, *** $p < 0.001$, **** $p < 0.0001$, ns = not significant). Standard error bars represent mean value with standard error. A total of 10,000 events were analyzed for each sample, $n = 3$. (D) MCPyV LT restricts cell proliferation by inducing senescence. Non–invasive live cell imaging of transduced BJ–hTERT cells was conducted using a phase holographic imaging system (HoloMonitor M4) to measure cell proliferation rates. (E) MCPyV LT inhibits cell proliferation. Cell proliferation assay. EdU incorporation (pink) was measured by fluorescence microscopy. Scale bar = 60 μm.

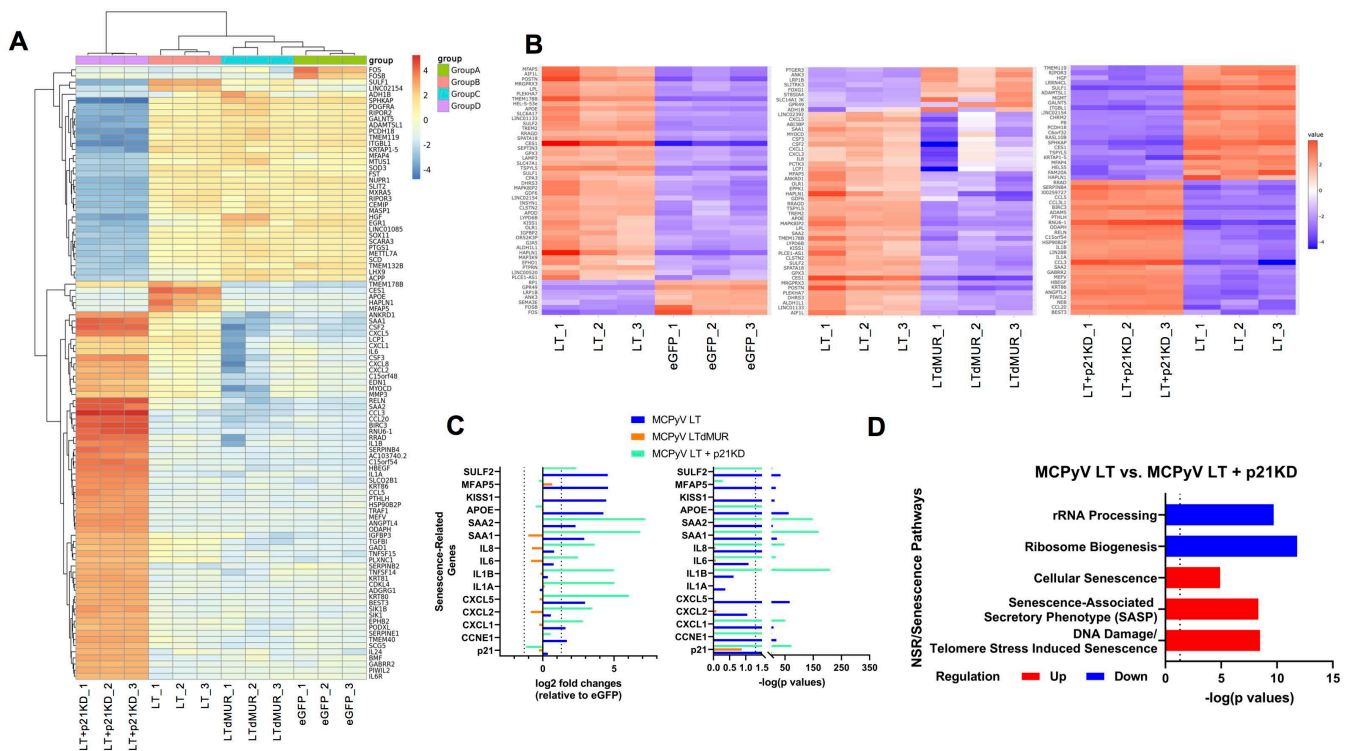


Figure 5. MCPyV LT-expressing cells are enriched in senescence-related genes. (A) Heatmap comparing top 100 differentially expressed genes, comparing eGFP, MCPyV LT, MCPyV LTdMUR, MCPyV LT+p21KD. (B) Heatmaps comparing the top 50 differentially expressed genes between MCPyV LT:eGFP (left), MCPyV LT:MCPyV LTdMUR (middle), MCPyV LT:MCPyV LT+p21KD (right). Heatmaps were generated using iDEP. (C) SASPs expression. Expression of senescence-related genes compared to eGFP empty vector cells. Log₂ fold changes (left): positive values represent upregulated genes compared to eGFP cells and negative values represent downregulated genes compared to eGFP cells. Vertical dashed lines represent ± 1.5 log₂ fold change with a false discovery rate (FDR) of 0.1. $-\log(p$ values) of senescence genes (right). Dotted line represents p value of 0.05, $-\log(0.05) = 1.3$. Abbreviations—*SULF2*: sulfatase 2, *MFAP5*; microfibril-associated protein 5; *KISS1*: kisspeptin 1; *APOE*: apolipoprotein E; *SAA*: serum amyloid A1 and A2; *IL*: interleukin, *CCNE1*: cyclin E1. (D) Senescence pathways enriched in MCPyV LT compared to MCPyV LT+p21KD. Dotted lines represent p value of 0.05, $-\log(0.05) = 1.3$ and p values to the right of the dotted line < 0.05 (significant).

2.6. MCPyV LT-Mediated Senescence Maintains MCPyV Genome

As senescent cells are characterized by a stable cell cycle arrest and are resistant to apoptosis [4], we asked if MCPyV could exploit cellular senescence to establish a persistent viral infection. To test the hypothesis that senescence is required for the longevity of MCPyV infection, and to do so in the context of an actual MCPyV molecular clone, we transfected BJ-hTERT cells with a full-length MCPyV genome (pMCPyV-MC) in which the early genes were tagged with eGFP-P2A (Figure 6A). Senescent MCPyV cells were present at 21 days post-transfection, whereas knockdown with p21 greatly abolished SA-β-gal staining (GFP⁺/SA-β-Gal⁺) as determined by both flow cytometry and microscopic analyses (Figures 6A,B and S9).

To determine if senescence is required for MCPyV genome maintenance, we reversely co-transfected BJ-hTERT cells with the MCPyV genome and scrambled shRNA lentiviral vector (mCherry-Puro shScr) or p21 shRNA vector (mCherry-Puro shp21.1). Cells were initially transfected with shp21.1 to inhibit senescence as we sought to determine how the loss of senescence impacts the long-term persistence of MCPyV. We observed MCPyV genome maintenance using flow cytometry by detecting GFP levels over time (Figure 6C). Because MCPyV LT induced G2 cell cycle arrest (Figure 4A), we specifically examined

the G2 population. Cells were gated on GFP and mCherry (GFP⁺mCherry⁺) to ensure that only cells that had taken up both MCPyV genome and shRNA plasmid were examined (Figure 6C). At day 14 post-transfection, p21 knockdown reduced the percentage of GFP⁺ (MCPyV⁺) cells by ~25% compared to scrambled control cells. Additionally, p21 knockdown could consistently reduce MCPyV genome levels at both 10- and 14-days post-transfection (Figure 6D), suggesting that MCPyV genome persistence is dependent on cellular senescence.

Previous studies have identified senolytics as drugs that can selectively clear senescent cells to reduce disease morbidity [1,10,45]. Therefore, we investigated whether senolytic treatment could potentially act as a therapeutic agent to prevent MCC. At fourteen days post-transfection, cells were treated with navitoclax, dasatinib and quercetin (D+Q), or DMSO for two days. To determine if these senolytics could reduce the senescent cell burden, a SA-β-Gal assay was conducted. Navitoclax treatment [46] could markedly reduce SA-β-Gal staining, whereas D+Q treatment did not show a significant change in SA-β-Gal staining (Figures 6E and S10). Moreover, navitoclax could reduce viral genomes levels, decreasing MCPyV DNA levels by ~70% (Figure 6F), demonstrating the importance of cellular senescence on MCPyV genome persistence.

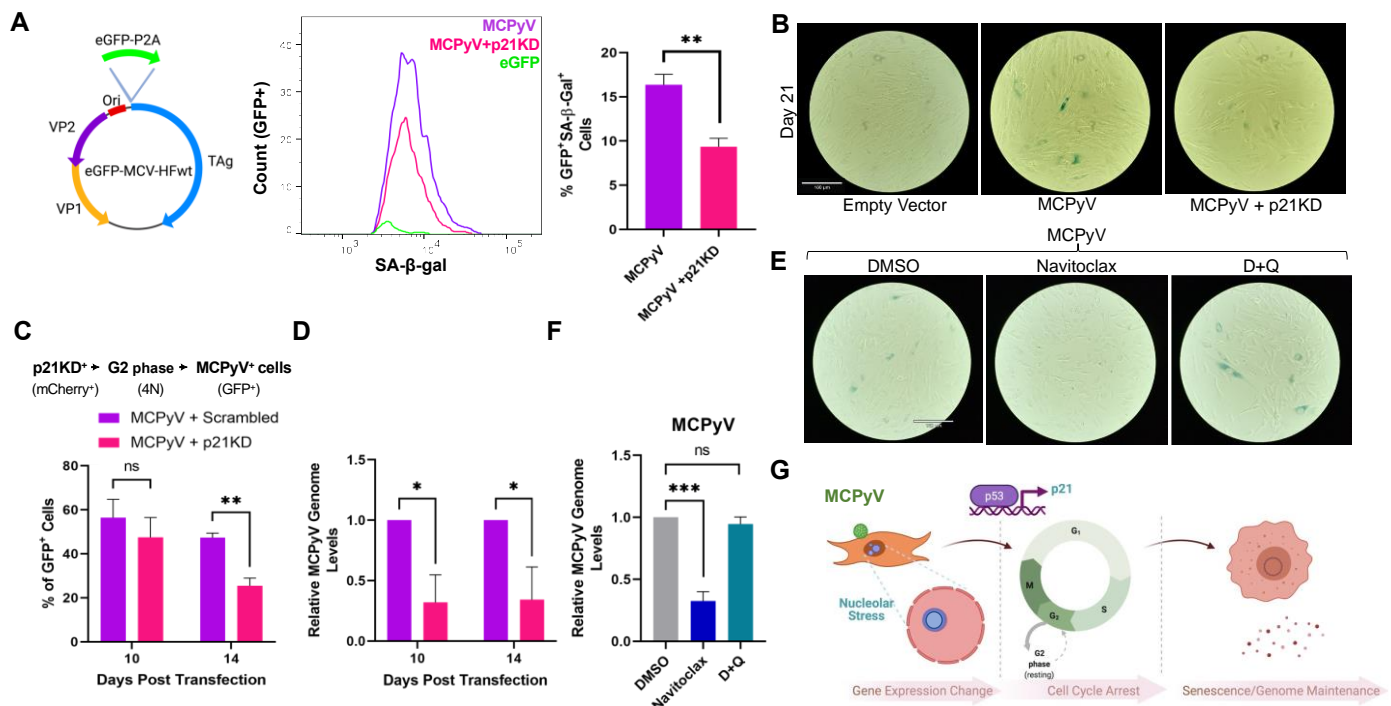


Figure 6. MCPyV-induced senescence is required for viral genome maintenance. (A) p21 knockdown decreases the percentage of senescent SA-β-gal⁺ cells. Schematic representing whole MCPyV genome construct encoding origin (Ori), VP1, VP2, T antigens (TAg), and eGFP-P2A (left). BJ-hTERT cells were reversely transfected with the MCPyV genome and then transduced with shp21.1 for p21 knockdown at 14 days post-transfection. At 21 days post-transfection, MCPyV-transfected cells were subjected to a senescence assay. Histogram representing GFP⁺/SA-β-gal⁺ (MCPyV⁺, senescent cells) for transfected MCPyV or MCPyV+p21KD cells (middle). Percentage of GFP⁺/SA-β-gal⁺ in population (right). Statistical significance was determined using unpaired Student’s *t*-test (** *p* < 0.01). Standard error bars represent mean value with standard error: n = 3; 10,000 cells recorded per replicate. (B) MCPyV-induced senescence is p21-dependent. Colorimetric SA-β-gal staining of MCPyV-transfected cells at 21 days post-transfection. (C) Cellular senescence maintains MCPyV genome. BJ-hTERT cells were co-transfected with MCPyV (GFP⁺) and mCherry-shScr or

mCherry–shp21.1 (p21KD, mCherry⁺). Cells were harvested at the stated days post–transfection and were analyzed by flow cytometry. Transfected cells were gated for mCherry⁺ (p21KD) cells and then examined for G2–arrested GFP⁺ cells (MCPyV⁺). Unpaired Student's *t*-test (ns = not significant). Standard error bars represent mean value with standard error, *n* = 3. (D) qPCR was conducted on cells reversely co–transfected with mCherry–shScr or mCherry–shp21.1, and MCPyV genome levels were reported at the given time points. Multiple unpaired Student's *t*-test (* *p* < 0.05). Standard error bars represent mean value with standard error, *n* = 3. (E) Senolytic treatment selectively clears MCPyV–induced senescent cells. At 14 days post–transfection, empty vector– or MCPyV–transfected cells were treated with navitoclax (250 nM), dasatinib and quercetin (D+Q, 25 nM dasatinib and 250 nM quercetin), or DMSO for two days, and then subjected to a SA–β–gal assay or qPCR (F). Scale bar = 180 μm. One–way ANOVA (***) *p* < 0.001. Standard error bars represent mean value with standard error, *n* = 3. (G) MCPyV induces senescence to sustain viral genome maintenance. MCPyV LT activates p53 and, subsequently, p21 through nucleolar stress responses. Activation of p21 induces G2 cell cycle arrest, leading to changes in growth arrest and senescent gene expression, as well as the promotion of cellular senescence. Cellular senescence establishes MCPyV infection in fibroblast cells, enabling it to extend its lifecycle within the host. Figure created with BioRender.com.

3. Discussion

Taken together, our results show that MCPyV infection, mainly MCPyV LT expression, can activate a nucleolar stress response in human fibroblast cells. This, in turn, activated p53 transcriptional activity, inducing p21 expression. p21 upregulation subsequently led to G2 cell cycle arrest, promoting cellular senescence. MCPyV was able to exploit these senescent cells by maintaining its viral genome for long-term survival (Figure 6G).

MCPyV-induced senescence was recently reported by Siebels et al. [20]. Although their MCPyV LT interaction study revealed an interaction with KRAB-associated protein 1 (KAP1), a senescence-related factor [47] in primary normal human dermal fibroblasts, Siebels et al. observed neither senescence nor p21 transcriptional activation assessed in primary nHDFs in 2–4 days of LT expression alone. Our data suggest that LT expression alone induces host cell senescence with significant morphologic changes in human fibroblasts, including BJ-hTERT (Figure 1), HFF-1, BJ, and nHDF (Figures S2A and S3A) at least 7 days post-transduction. An upregulation of p21 was also observed in neonatal nHDF cells at 10 days post-transduction (Figure S3B). These data suggest that MCPyV LT expression alone can gradually promote cellular senescence at later time points (≥7 days post-transduction). As an unexpected high SA–β–gal-positive background was observed in early passages of non-immortalized skin fibroblast cells (Figures S2B and S3C), we used BJ-hTERT, a skin fibroblast cell line commonly used to study aging and senescence [48–50], for all our experiments to determine accurate gene changes in MCPyV LT-induced senescence. Although BJ-hTERT cells express human telomerase reverse transcriptase (hTERT), which is known to inhibit senescence, it has been shown that hTERT has no effect on stress-induced senescence [51], but only inhibits stress-related apoptosis and necrosis [52].

In a latent viral infection, while the full viral genome is retained in the host cell, its late gene expression is dramatically restricted and only few viral antigens and no viral particles are produced. To qualify as latency, this quiescent state of infection must display persistence and reversibility [53]. Protein-mediated viral latency is the only known mechanism for human polyomavirus latency, shown by successful reversibility from a quiescent state to a productive infection that is regulated by MCPyV LT proteostasis [17]. Accompanied by protein interaction networks [15,17,20,54], we show that an additional key nucleolar stress pathway, triggered by MCPyV LT overexpression, plays a pivotal role in persistent viral infection.

Although viral replicative machinery has been associated with modulating the nucleolus function, very few DNA viral oncoproteins have been specifically characterized to trigger changes in nucleolar distribution [38,55]. Canonically, the induction of the nucleolar stress response is caused by a disruption of ribosomal biogenesis [32]. Though our RNA-

Seq data suggest MCPyV LT can downregulate rRNA synthesis, the mechanism of NSR induction by MCPyV LT needs further investigation. Certainly, other stress responses in different cell types, such as DDR, shortened telomeres, replicative stresses, and/or apoptosis, will combinedly influence the extent of senescence in the early and late stages of the infection process. Nonetheless, it is important that both persistency and reversibility are mainly modulated by the MCPyV LT unique domain that is potentially involved in a series of host interactions and the regulation of its own proteostasis [15,17,56,57].

Most of the known human cancer viruses have the ability to antagonize p53 by expressing viral oncoproteins that promote cellular proliferation by abrogating p53-induced cell cycle arrest in response to DNA damage [58]. Human polyomavirus LTs have been known to interact with p53, which immediately blocks DDR and innate immune sensing for the host's survival in the initial infection process [59]. Unlike other human polyomaviruses, MCPyV LT does not seem to possess the ability to interact and directly inhibit p53 [14], but rather activate p53 phosphorylation and function [13]. This activation of p21 transcription by p53, uniquely induced by MCPyV LT, may establish a distinct niche of MCPyV as a human-cancer-causing virus among human polyomaviruses. Low mutation rates of p53 [54,60] and an intact p53/p21 pathway [61] in MCCs consistently support our results that the activation of p21-dependent senescence potentially plays a role in MCPyV infection.

It should be noted that the LT-induced senescence response in human fibroblasts has been simultaneously evolving throughout the passage of time, potentially due to changes in miRNA and gene expression profiles [62], suggesting a variety of gene expression changes can alter and allow host cellular responses to support latent infection periods. Specifically, we observed that late passages of BJ-hTERT cells supported enhanced senescence and reduced cell death with LT expression and p21 knockdown conditions compared to early passaged cells. We also noticed a significant level of mitotic cell death as an early event induced by p21 knockdown, although cells recover over time. This p21 knockdown-mediated cell death may be caused by the re-entry of senescent cells back into the cell cycle, which enhances the activation of DDR as shown by others [63].

Senescence has been characterized as an irreversible exit of the cell cycle [64]. Given that certain viruses depend on host cell proliferation for viral replication, viral oncogene-mediated cell senescence has been suggested to be an antiviral mechanism for host cells. Our results define a central role of senescence as a potential contributing factor to viral oncogenesis that has not been previously described. Despite this cell-intrinsic tumor suppression, senescent cells have also been implicated as active contributors to tumorigenesis by extrinsically promoting many hallmarks of cancer, including evasion of the immune system [65]. Through the induction of cellular senescence, MCPyV potentially creates a precancerous environment in which it can avoid the immune system that enhances cell survival and viral persistence. The senolytic drug navitoclax is a Bcl-2 anti-apoptotic family protein inhibitor. Early studies on navitoclax have shown promising results to suppress MCC growth [66,67], suggesting the Bcl-2 pathway as a potential therapeutic target to prevent MCPyV infection and MCC development. Because senescent cells are heterogeneous [1], senolytics that utilize different mechanisms of action are able to target senescent cells and the detrimental effects of navitoclax on LT-related cellular senescence remain to be further investigated.

Although whether latent viral infection can ultimately lead to oncogenesis by inducing host senescence and other stress environments needs further investigation, such cellular responses surely contribute to maintaining cellular homeostasis during virus infections. Our results uncover the mechanism of a host stress response in regulating human polyomavirus genome maintenance in a persistent viral infection, which may lead to targeted interventions for MCC.

4. Materials and Methods

4.1. Cell Culture and Plasmids

BJ-hTERT (ATCC, RRID:CVCL_6573) and 293FT cells (Invitrogen, RRID:CVCL_6911, Rockford, IL, USA) were cultured in Dulbecco's modified Eagle's medium (DMEM) with 10% premium grade fetal bovine serum (FBS, Seradigm). HFF-1 (ATCC, RRID:CVCL_3285) and BJ (ATCC, RRID:CVCL_3653) cells were grown in 15% FBS in DMEM. Fibroblast growth basal medium (FBM, Lonza, Walkersville, MD, USA) or fibroblast growth medium (Sigma-Aldrich, Milwaukee, WI, USA) was used to culture neonatal primary normal human dermal fibroblast cells (Lonza). BJ-hTERT, BJ, and HFF-1 cell lines were kindly provided by Dr. Chang and Dr. Moore. Plasmid constructs encoding codon-optimized cDNA for MCPyV LT, MCPyV LTdMUR, SV40 LT, and SV40 LT+MUR were cloned into pLVX-GFP-P2A empty vectors as previously described [15]. Enhanced GFP (eGFP) was cloned into MCPyV genome (pMCPyV-MC) to visualize MCPyV early gene expression (Figure S11).

4.2. Lentiviral Transduction and p21 Knockdown

For lentivirus production, 293FT cells (Invitrogen) were co-transfected with lentiviral psPAX2 packaging, pMD2.G envelop, and pLVX or pLKO.1 transfer plasmids (Addgene, Watertown, MA, USA) using jetOPTIMUS (Polyplus Transfection, New York, NY, USA) according to the manufacturer's instructions, except the amounts of each plasmid were increased for optimal lentiviral production. Cells were transduced with a lentivirus encoding pLVX-GFP-P2A empty vector, MCPyV LT, MCPyV LTdMUR, SV40 LT, or SV40 LT+MUR in the presence of 6 µg/mL polybrene (Sigma-Aldrich, St. Louis, MO, USA). Stably transduced cells were selected and maintained with 3 µg/mL puromycin (Sigma-Aldrich). MCPyV LT-expressing BJ-hTERT cells were grown for 14 days and then transduced with scrambled (Scr) short hairpin RNA (shRNA), shp21.1, shp21.2, or both shp21.1/2 for p21 knockdown analysis. shRNA sequences of p21 (shp21.1: TRCN0000287021, shp21.2: TRCN0000040126) were cloned into lentiviral vector pLKO.1 neo (Addgene#13425) or pLKO.1 mCherry-Puro generated by overlapping PCR using primer pairs (Table S1) using AgeI and EcoRI. After transduction, cells were selected with 500 µg/mL geneticin (G418, Gibco, Rockford, IL, USA) for two days. Knockdown efficiency was confirmed by reverse transcription-quantitative PCR (RT-qPCR) using the p21 primer pairs listed in Table S1 and immunoblots seven days after p21 knockdown (21 days post-transduction). All experiments were conducted after 14 days (without p21 knockdown) or 21 days post-transduction (with p21 knockdown).

4.3. Quantitative Immunoblotting and Antibodies

Stably transduced BJ-hTERT cells (selected with puromycin for 14 days) were lysed with an IP buffer (50 mM Tris-HCl (pH 8.0), 150 mM NaCl, 1% TritonX-100, 1 mM PMSF, 1 mM benzamidine) and whole cell lysates were used for immunoblot analyses. Membranes were incubated with a primary antibody overnight at 4 °C, and then incubated with a secondary antibody for 2 h (h) at room temperature (RT). A quantitative infrared (IR) imaging system, Odyssey CLX (LI-COR), was used to determine protein expression. The primary antibodies used in this study included phospho-p53 (Ser15) (Cell Signaling, 9284, Danvers, MA, USA), p21 Waf1/Cip1 (Cell Signaling, 2947), cyclin E (Santa Cruz Biotechnology, sc-247, Dallas, TX, USA), phospho-histone H3 (Ser10) (Cell Signaling, 53348), GFP (Santa Cruz Biotechnology, sc-9996), and β-Actin (Cell Signaling, 4970). All signals were detected using quantitative infrared (IR) secondary antibodies (IRDye 800CW goat anti-mouse, 800CW goat anti-rabbit, 680LT goat anti-rabbit IgG, 680LT goat anti-mouse IgG) (LI-COR).

4.4. Immunofluorescence Assay

Transduced BJ-hTERT or neonatal nHDF cells were seeded in 6-well plates or 8-well chamber slides (Nunc™ Lab-Tek™, Sigma-Aldrich). Cells were fixed in 4% paraformaldehyde in PBS (Alfa Aesar) for 10 min and then permeabilized in 1% Triton X-100 (Sigma-Aldrich) in PBS for 20 min. In PBS, 3% BSA/0.1 M glycine was used to block for 1 h. Cells

were incubated overnight at 4 °C with the following primary antibodies: γ -H2AX(Ser139) (Cell Signaling, 9718); p21 Waf1/Cip1 (Cell Signaling, 2947); pHH3 (Cell Signaling, 53348); p-p53(S15) (Cell Signaling, 9284); and NPM1 (FC-61991, Life Technologies). Secondary antibody (A11029 or A11036, Alexa Fluor 568-conjugated goat anti-mouse or anti-rabbit IgG (HL) Highly Cross-Adsorbed, Invitrogen) was used to stain cells for 1 h. Cells were incubated with DAPI (0.1 μ g/mL, Thermo Scientific, Rockford, IL, USA) for 5 min and then analyzed by fluorescence imaging using a REVOLVE4 microscope (Echo Laboratories, San Diego, CA, USA).

4.5. Senescence Assay

The detection of SA- β -Gal activity was performed using a colorimetric senescence β -Galactosidase histochemical staining kit (G-Biosciences, St. Louis, MO, USA) or a fluorescent Cell Meter™ Cellular Senescence Activity Assay Kit with Xite™ Red beta-D-galactopyranoside (AAT Bioquest, Pleasanton, CA, USA) according to the manufacturer's instructions. Briefly, the cells were washed with cold PBS and then fixed with 4% paraformaldehyde in PBS for 15 min. Cells were then permeabilized for 15 min with 0.1% Triton in PBS or a permeabilization buffer (Thermo Scientific, Rockford, IL, USA). After incubation with the SA- β -Gal detection solution for 12 h (G-Biosciences) or 45 min (AAT Bioquest) at 37 °C, the cells were stained with DAPI (Thermo Scientific) for microscopic analyses or Hoechst 33342 (Invitrogen) for flow cytometric analyses. For LT-transduced BJ-hTERT cells, senescence assays were performed at 14 days or 21 days post-transduction for samples with or without p21 knockdown, respectively. Normal and primary fibroblast cell lines were stained for SA- β -Gal at 7 days post-transduction. MCPyV genome-transfected cells were transduced with shp21.1 at 14 days post-transfection. At 21 days post-transfection, a senescence assay was conducted. Images were captured using a REVOLVE4 fluorescent microscope (Echo Laboratories). All the samples were stained at least in triplicate. A total of 50 cells were counted for each LT construct. The nuclear area was calculated using Echo Pro software (Echo Laboratories). A positive PE signal was detected using the PE-Annexin V (BD Biosciences, San Jose, CA, USA) or CS&T Research Beads (BD Biosciences, 655050). For PE-positive control samples, BJ-hTERT cells were washed twice with PBS and then heat-killed by incubation at 95 °C for 3 min. A 1:1 cell suspension of heat-killed and non-heat-killed cells were stained according to the manufacturer's instructions. A total of 10,000 events were recorded in triplicate for each sample.

4.6. SASP Analysis by RT-qPCR

For RT-qPCR, total RNA was isolated using the Monarch Total RNA Miniprep Kit (New England Biolabs, Ipswich, MA, USA) according to the manufacturer's instructions. mRNA levels of SASPs (Figure 1E) were measured by RT-qPCR using an iTaq Universal One-Step RT-qPCR Kit (Bio-Rad, Hercules, CA, USA) with primer pairs as previously described [68]. Quantitative analyses were performed using the comparative $\Delta\Delta$ Ct method by detecting ribonuclease P (*RNase P*) and glyceraldehyde 3-phosphate dehydrogenase (*GAPDH*) as reference genes using the primer pairs listed in Table S1. All RT-qPCR experiments included melting curve analyses to confirm the specificity of the amplicons (95 °C for 15 s, 60 °C for 20 s, and 95 °C for 15 s).

4.7. Cell Cycle Analysis

BJ-hTERT cells were fixed, permeabilized, and then stained with Hoechst 33342 (Invitrogen) to determine cell cycle stages. Cells were analyzed using an LSR Fortessa flow cytometer (BD Biosciences) and 10,000 events were recorded per replicate. FlowJo (TreeStar, Ashland, OR, USA) software was utilized for data analyses. To examine viable cells, forward scatter (FSC) area versus the side scatter (SSC) area density plots were analyzed. Doublets were removed through the FSC area versus the FSC height gating. Cell cycle analyses were conducted on GFP-positive cells to examine only the transduced cells.

4.8. EdU Incorporation Assay

Cells were pulse labelled with EdU (final concentration of 10 μ M, Invitrogen) 24 h before fixation. EdU incorporation was detected using the Click-iT Plus EdU Alexa 647 Fluor Imaging Kit (Invitrogen) according to the manufacturer's instructions. Cells were then stained with DAPI (Thermo Scientific) and visualized with a fluorescence microscope (REVOLVE4, Echo Laboratories).

4.9. Cell Proliferation Assay

Cells were plated on 6-well, TC plates (Thermo Scientific) at a confluency of approximately 30%, and they were incubated with 10% serum. After 24 h, cells were recorded using a phase holographic imaging system (HoloMonitor M4 laser microscope, Phase Holographic Imaging, Lund, Sweden) [37]. Images were recorded every 30 min for 48 h. Average cell proliferation was quantified using HStudio M4 software (version 2.7.1).

4.10. RNA Sequencing Analysis

RNA sequencing and gene reads were aligned to the hg38 human genome. Raw gene counts were used for integrated differential expression and pathway (iDEP) analyses and were transformed and normalized using iDEP [69]. All figures and sequence analyses were generated from iDEP or Zymo Research. Genes below 0.5 counts per million (CPM) were excluded and the false-discovery rate (FDR) for differential gene expression was kept below 0.1 (FDR < 0.1) with a minimum fold change of 1.5. RNA sequence data are available at the NCBI Gene Expression Omnibus (GEO) under the following accession number: GSE189291.

4.11. Flow Cytometric Analysis of MCPyV Genome

The MCPyV genome [70] with eGFP (pMCPyV-MC, Figure S11) was inserted into a minicircle (MC) parental backbone plasmid pTubb3-MC (Addgene #87112) using SmaI/BsrGI/BstEI sites and isolated according to the manufacturer's instructions (System Biosciences, Palo Alto, CA, USA). BJ-hTERT cells were reverse-transfected with pMCPyV-MC and either mCherry-Puro shScr or mCherry-Puro shp21.1 to inhibit senescence and to determine its impact on long-term viral maintenance. At 10- and 14-days post-transfection, cells were harvested and subjected to flow cytometry to measure GFP and mCherry levels. The detection of mCherry indicated the expression of p21 shRNA constructs and the observation of GFP indicated the presence of the MCPyV genome. Cells were first gated on mCherry, which was followed by the gating of GFP to ascertain how p21 knockdown affected MCPyV persistence. The gating of GFP and then mCherry was used to ensure MCPyV-infected cells had taken up shRNA constructs. MCPyV viral genome levels of BJ-hTERT reversely co-transfected with mCherry-Puro shScr or mCherry-Puro shp21.1 were also calculated utilizing qPCR with 20 ng of DpnI digested DNA, isolated using Quick-DNA kit (Zymo Research, Irvine, CA, USA). qPCR was carried out with PowerUpTM SYBR Green Master Mix (Applied Biosystems, Foster City, CA, USA) using a StepOnePlusTM system (Applied Biosystems) according to the manufacturer's protocol. Quantitative analyses were performed using the comparative $\Delta\Delta$ Ct method by detecting *RNase P* as a reference gene and three MCPyV detection primer pairs (Table S1). All qPCR experiments included melting curve analyses to confirm the specificity of the amplicons (95 °C for 15 s, 60 °C for 20 s, and 95 °C for 15 s).

4.12. Senolytic Treatment

pMCPyV-MC or pTubb3-MC (Addgene #87112) transfected cells were maintained for 14 days to yield the establishment of senescent phenotypes. Cells were plated onto 24-well or 12-well plates for the SA- β -Gal assay or qPCR analysis, respectively, and grown for one day. Navitoclax (250 nM), D+Q (25 nM dasatinib plus 250 nM quercetin) (Selleckchem), or DMSO (Sigma-Aldrich) were added to the cells for two days. Senolytic-treated cells were then subjected to a SA- β -Gal assay or qPCR to detect viral genome levels, in which 25 ng of undigested DNA was analyzed.

4.13. Statistical Analysis

The figures show the average values and the error bars show the standard error or standard deviation. One-way analysis of variance (ANOVA), multiple Student's *t*-tests, or unpaired Student's *t*-test was used to determine statistical significance, with $p < 0.05$ considered significant using GraphPad Prism software (GraphPad Software, Inc., La Jolla, CA, USA). Unless stated, all experiments were tested at least three times.

Supplementary Materials: The following supporting information can be downloaded at <https://www.mdpi.com/article/10.3390/cells12030380/s1> Figure S1: MCPyV LT alters expression of growth arrest genes; Figure S2: MCPyV LT expression exhibits senescence-specific enlarged nucleus in HFF-1 and BJ foreskin fibroblasts; Figure S3: MCPyV LT expression promotes senescent phenotypes in neonatal normal primary dermal fibroblast cells; Figure S4: Immunofluorescent analysis of γ -H2AX; Figure S5: MCPyV LT induces p21-dependent senescence; Figure S6: MCPyV LT expression induces G2 cell cycle arrest; Figure S7: MCPyV LT negatively regulates cell growth by inducing cellular senescence; Figure S8: Differential gene expression analysis; Figure S9: MCPyV induces p21-dependent senescence; Figure S10: Senolytic treatment inhibits MCPyV-induced cellular senescence; Figure S11: MCPyV minicircle genome; Table S1: Primers used in this study; Supplementary Dataset S1.

Author Contributions: Conceptualization, A.M.P. and H.J.K.; methodology, A.M.P., L.E.O., A.E.L. and H.J.K.; visualization, A.M.P., L.E.O. and H.J.K.; formal analysis, A.M.P., L.E.O. and H.J.K.; writing—original draft, A.M.P. and H.J.K.; writing—review and editing, A.M.P., L.E.O., A.E.L. and H.J.K.; supervision, H.J.K. All authors have read and agreed to the published version of the manuscript.

Funding: This project is funded, in part, under a grant with the Pennsylvania Department of Health using Tobacco CURE Funds (SAP# 4100083097). The Department specifically disclaims responsibility for any analyses, interpretations or conclusions (H.J.K.). A.E.L. is supported by the National Institutes of Health grant 1R35NS127217.

Institutional Review Board Statement: Not applicable.

Informed Consent Statement: Not applicable.

Data Availability Statement: All data generated in this study are presented in the paper, supplementary information, supplementary dataset, and NCBI GEO (accession number GSE189291).

Acknowledgments: We thank the Department of Microbiology and Immunology and flow cytometry core at Penn State College of Medicine (RRID:SCR_021134) for their support in this project. We also thank Zachary Flegal for assistance with the holographic imaging data analysis, Nnenna Nwogu for preliminary work, and John Tawil for repeating and confirming qPCR results.

Conflicts of Interest: The authors declare no conflict of interest.

References

1. Di Micco, R.; Krizhanovsky, V.; Baker, D.; d'Adda di Fagagna, F. Cellular senescence in ageing: From mechanisms to therapeutic opportunities. *Nat. Rev. Mol. Cell Biol.* **2021**, *22*, 75–95. [[CrossRef](#)] [[PubMed](#)]
2. Baz-Martínez, M.; Da Silva-Álvarez, S.; Rodríguez, E.; Guerra, J.; El Motiam, A.; Vidal, A.; García-Caballero, T.; González-Barcia, M.; Sánchez, L.; Muñoz-Fontela, C.; et al. Cell senescence is an antiviral defense mechanism. *Sci. Rep.* **2016**, *6*, 37007. [[CrossRef](#)] [[PubMed](#)]
3. van Deursen, J.M. The role of senescent cells in ageing. *Nature* **2014**, *509*, 439–446. [[CrossRef](#)] [[PubMed](#)]
4. Herranz, N.; Gil, J. Mechanisms and functions of cellular senescence. *J. Clin. Invest.* **2018**, *128*, 1238–1246. [[CrossRef](#)] [[PubMed](#)]
5. Kelley, W.J.; Zemans, R.L.; Goldstein, D.R. Cellular senescence: Friend or foe to respiratory viral infections? *Eur. Respir. J.* **2020**, *56*, 2002708. [[CrossRef](#)] [[PubMed](#)]
6. Kim, J.A.; Seong, R.K.; Shin, O.S. Enhanced Viral Replication by Cellular Replicative Senescence. *Immune Netw.* **2016**, *16*, 286–295. [[CrossRef](#)]
7. Seoane, R.; Vidal, S.; Bouzaher, Y.H.; El Motiam, A.; Rivas, C. The Interaction of Viruses with the Cellular Senescence Response. *Biology* **2020**, *9*, 455. [[CrossRef](#)] [[PubMed](#)]
8. Chuprin, A.; Gal, H.; Biron-Shental, T.; Biran, A.; Amiel, A.; Rozenblatt, S.; Krizhanovsky, V. Cell fusion induced by ERVWE1 or measles virus causes cellular senescence. *Genes Dev.* **2013**, *27*, 2356–2366. [[CrossRef](#)]
9. Hsieh, T.H.; Tsai, T.T.; Chen, C.L.; Shen, T.J.; Jhan, M.K.; Tseng, P.C.; Lin, C.F. Senescence in Monocytes Facilitates Dengue Virus Infection by Increasing Infectivity. *Front. Cell. Infect. Microbiol.* **2020**, *10*, 375. [[CrossRef](#)]

10. Camell, C.D.; Yousefzadeh, M.J.; Zhu, Y.; Prata, L.G.P.L.; Huggins, M.A.; Pierson, M.; Zhang, L.; O’Kelly, R.D.; Pirtskhalava, T.; Xun, P.; et al. Senolytics reduce coronavirus-related mortality in old mice. *Science* **2021**, *373*, eabe4832. [[CrossRef](#)]
11. Chang, Y.; Moore, P.S. Merkel cell carcinoma: A virus-induced human cancer. *Annu Rev. Pathol.* **2012**, *7*, 123–144. [[CrossRef](#)] [[PubMed](#)]
12. Kwun, H.J.; Guastafierro, A.; Shuda, M.; Meinke, G.; Bohm, A.; Moore, P.S.; Chang, Y. The minimum replication origin of merkel cell polyomavirus has a unique large T-antigen loading architecture and requires small T-antigen expression for optimal replication. *J. Virol.* **2009**, *83*, 12118–12128. [[CrossRef](#)] [[PubMed](#)]
13. Li, J.; Wang, X.; Diaz, J.; Tsang, S.H.; Buck, C.B.; You, J. Merkel cell polyomavirus large T antigen disrupts host genomic integrity and inhibits cellular proliferation. *J. Virol.* **2013**, *87*, 9173–9188. [[CrossRef](#)] [[PubMed](#)]
14. Cheng, J.; Rozenblatt-Rosen, O.; Paulson, K.G.; Nghiem, P.; DeCaprio, J.A. Merkel cell polyomavirus large T antigen has growth-promoting and inhibitory activities. *J. Virol.* **2013**, *87*, 6118–6126. [[CrossRef](#)] [[PubMed](#)]
15. Nwogu, N.; Ortiz, L.E.; Kwun, H.J. Merkel Cell Polyomavirus Large T Antigen Unique Domain Regulates Its Own Protein Stability and Cell Growth. *Viruses* **2020**, *12*, 1043. [[CrossRef](#)]
16. Houben, R.; Angermeyer, S.; Haferkamp, S.; Aue, A.; Goebeler, M.; Schrama, D.; Hesbacher, S. Characterization of functional domains in the Merkel cell polyoma virus Large T antigen. *Int. J. Cancer* **2015**, *136*, E290–E300. [[CrossRef](#)]
17. Kwun, H.J.; Chang, Y.; Moore, P.S. Protein-mediated viral latency is a novel mechanism for Merkel cell polyomavirus persistence. *Proc. Natl. Acad. Sci. USA* **2017**, *114*, E4040–E4047. [[CrossRef](#)]
18. Ortiz, L.E.; Pham, A.M.; Kwun, H.J. Identification of the Merkel Cell Polyomavirus Large Tumor Antigen Ubiquitin Conjugation Residue. *Int. J. Mol. Sci.* **2021**, *22*, 7169. [[CrossRef](#)]
19. Kwun, H.J.; Shuda, M.; Feng, H.; Camacho, C.J.; Moore, P.S.; Chang, Y. Merkel cell polyomavirus small T antigen controls viral replication and oncoprotein expression by targeting the cellular ubiquitin ligase SCFFbw7. *Cell Host Microbe* **2013**, *14*, 125–135. [[CrossRef](#)]
20. Siebels, S.; Czech-Sioli, M.; Spohn, M.; Schmidt, C.; Theiss, J.; Indenbirken, D.; Günther, T.; Grundhoff, A.; Fischer, N. Merkel Cell Polyomavirus DNA Replication Induces Senescence in Human Dermal Fibroblasts in a Kap1/Trim28-Dependent Manner. *mBio* **2020**, *11*, e00142-20. [[CrossRef](#)]
21. Moran, J.M.T.; Biecek, P.; Donizy, P.; Wu, C.L.; Kopczynski, J.; Pieniazek, M.; Ryś, J.; Hoang, M.P. Large nuclear size correlated with better overall survival, Merkel cell polyomavirus positivity, and terminal deoxynucleotidyl transferase expression in Merkel cell carcinoma. *J. Am. Acad. Dermatol.* **2021**, *84*, 550–552. [[CrossRef](#)] [[PubMed](#)]
22. Mazumder, S.; DuPree, E.L.; Almasan, A. A dual role of cyclin E in cell proliferation and apoptosis may provide a target for cancer therapy. *Curr. Cancer Drug Targets* **2004**, *4*, 65–75. [[CrossRef](#)] [[PubMed](#)]
23. Koff, A.; Cross, F.; Fisher, A.; Schumacher, J.; Leguellec, K.; Philippe, M.; Roberts, J.M. Human cyclin E, a new cyclin that interacts with two members of the CDC2 gene family. *Cell* **1991**, *66*, 1217–1228. [[CrossRef](#)] [[PubMed](#)]
24. Dulić, V.; Lees, E.; Reed, S.I. Association of human cyclin E with a periodic G1-S phase protein kinase. *Science* **1992**, *257*, 1958–1961. [[CrossRef](#)] [[PubMed](#)]
25. Dulić, V.; Drullinger, L.F.; Lees, E.; Reed, S.I.; Stein, G.H. Altered regulation of G1 cyclins in senescent human diploid fibroblasts: Accumulation of inactive cyclin E-Cdk2 and cyclin D1-Cdk2 complexes. *Proc. Natl. Acad. Sci. USA* **1993**, *90*, 11034–11038. [[CrossRef](#)]
26. Van Hooser, A.; Goodrich, D.W.; Allis, C.D.; Brinkley, B.R.; Mancini, M.A. Histone H3 phosphorylation is required for the initiation, but not maintenance, of mammalian chromosome condensation. *J. Cell Sci.* **1998**, *111*, 3497–3506. [[CrossRef](#)]
27. Ren, J.; Tang, C.Z.; Li, X.D.; Niu, Z.B.; Zhang, B.Y.; Zhang, T.; Gao, M.J.; Ran, X.Z.; Su, Y.P.; Wang, F.C. Identification of G2/M phase transition by sequential nuclear and cytoplasmic changes and molecular markers in mice intestinal epithelial cells. *Cell Cycle* **2018**, *17*, 780–791. [[CrossRef](#)]
28. Hendzel, M.J.; Wei, Y.; Mancini, M.A.; Van Hooser, A.; Ranalli, T.; Brinkley, B.R.; Bazett-Jones, D.P.; Allis, C.D. Mitosis-specific phosphorylation of histone H3 initiates primarily within pericentromeric heterochromatin during G2 and spreads in an ordered fashion coincident with mitotic chromosome condensation. *Chromosoma* **1997**, *106*, 348–360. [[CrossRef](#)]
29. Guo, C.Y.; Mizzen, C.; Wang, Y.; Larner, J.M. Histone H1 and H3 dephosphorylation are differentially regulated by radiation-induced signal transduction pathways. *Cancer Res.* **2000**, *60*, 5667–5672.
30. Rogakou, E.P.; Pilch, D.R.; Orr, A.H.; Ivanova, V.S.; Bonner, W.M. DNA double-stranded breaks induce histone H2AX phosphorylation on serine 139. *J. Biol. Chem.* **1998**, *273*, 5858–5868. [[CrossRef](#)]
31. Rubbi, C.P.; Milner, J. Disruption of the nucleolus mediates stabilization of p53 in response to DNA damage and other stresses. *EMBO J.* **2003**, *22*, 6068–6077. [[CrossRef](#)] [[PubMed](#)]
32. Yang, K.; Yang, J.; Yi, J. Nucleolar Stress: Hallmarks, sensing mechanism and diseases. *Cell Stress* **2018**, *2*, 125–140. [[CrossRef](#)] [[PubMed](#)]
33. Yang, K.; Wang, M.; Zhao, Y.; Sun, X.; Yang, Y.; Li, X.; Zhou, A.; Chu, H.; Zhou, H.; Xu, J.; et al. A redox mechanism underlying nucleolar stress sensing by nucleophosmin. *Nat. Commun.* **2016**, *7*, 13599. [[CrossRef](#)] [[PubMed](#)]
34. Potapova, T.A.; Gerton, J.L. Ribosomal DNA and the nucleolus in the context of genome organization. *Chromosome Res.* **2019**, *27*, 109–127. [[CrossRef](#)] [[PubMed](#)]
35. Gallardo, P.; Real-Calderón, P.; Flor-Parra, I.; Salas-Pino, S.; Daga, R.R. Acute Heat Stress Leads to Reversible Aggregation of Nuclear Proteins into Nucleolar Rings in Fission Yeast. *Cell Rep.* **2020**, *33*, 108377. [[CrossRef](#)] [[PubMed](#)]

36. Hein, J.; Boichuk, S.; Wu, J.; Cheng, Y.; Freire, R.; Jat, P.S.; Roberts, T.M.; Gjoerup, O.V. Simian virus 40 large T antigen disrupts genome integrity and activates a DNA damage response via Bub1 binding. *J. Virol.* **2009**, *83*, 117–127. [[CrossRef](#)]
37. Mölder, A.; Sebesta, M.; Gustafsson, M.; Gisselson, L.; Wingren, A.G.; Alm, K. Non-invasive, label-free cell counting and quantitative analysis of adherent cells using digital holography. *J. Microsc.* **2008**, *232*, 240–247. [[CrossRef](#)]
38. Iarovaia, O.V.; Minina, E.P.; Sheval, E.V.; Onichtchouk, D.; Dokudovskaya, S.; Razin, S.V.; Vassetzky, Y.S. Nucleolus: A Central Hub for Nuclear Functions. *Trends Cell. Biol.* **2019**, *29*, 647–659. [[CrossRef](#)]
39. Paluvai, H.; Di Giorgio, E.; Brancolini, C. The Histone Code of Senescence. *Cells* **2020**, *9*, 466. [[CrossRef](#)]
40. Chau, B.N.; Diaz, R.L.; Saunders, M.A.; Cheng, C.; Chang, A.N.; Warren, P.; Bradshaw, J.; Linsley, P.S.; Cleary, M.A. Identification of SULF2 as a novel transcriptional target of p53 by use of integrated genomic analyses. *Cancer Res.* **2009**, *69*, 1368–1374. [[CrossRef](#)]
41. Voutetakis, K.; Chatziioannou, A.; Gonos, E.S.; Trougakos, I.P. Comparative Meta-Analysis of Transcriptomics Data during Cellular Senescence and In Vivo Tissue Ageing. *Oxid. Med. Cell Longev.* **2015**, *2015*, 732914. [[CrossRef](#)] [[PubMed](#)]
42. Franceschini, I.; Desroziers, E. Development and Aging of the Kisspeptin-GPR54 System in the Mammalian Brain: What are the Impacts on Female Reproductive Function? *Front. Endocrinol.* **2013**, *4*, 22. [[CrossRef](#)] [[PubMed](#)]
43. Fernandez, C.G.; Hamby, M.E.; McReynolds, M.L.; Ray, W.J. The Role of APOE4 in Disrupting the Homeostatic Functions of Astrocytes and Microglia in Aging and Alzheimer’s Disease. *Front. Aging Neurosci.* **2019**, *11*, 14. [[CrossRef](#)]
44. Nishimura, K.; Taguchi, K.; Kishi, S.; Brooks, C.R.; Ochi, A.; Kadoya, H.; Ikeda, Y.; Miyoshi, M.; Tamaki, M.; Abe, H.; et al. Dual disruption of eNOS and ApoE gene accelerates kidney fibrosis and senescence after injury. *Biochem. Biophys. Res. Commun.* **2021**, *556*, 142–148. [[CrossRef](#)]
45. Lee, S.; Yu, Y.; Trimpert, J.; Benthani, F.; Mairhofer, M.; Richter-Pechanska, P.; Wyler, E.; Belenki, D.; Kaltenbrunner, S.; Pammer, M.; et al. Virus-induced senescence is a driver and therapeutic target in COVID-19. *Nature* **2021**, *599*, 283–289. [[CrossRef](#)]
46. Zhu, Y.; Tchkonja, T.; Fuhrmann-Stroissnigg, H.; Dai, H.M.; Ling, Y.Y.; Stout, M.B.; Pirtskhalava, T.; Giorgadze, N.; Johnson, K.O.; Giles, C.B.; et al. Identification of a novel senolytic agent, navitoclax, targeting the Bcl-2 family of anti-apoptotic factors. *Aging Cell* **2016**, *15*, 428–435. [[CrossRef](#)] [[PubMed](#)]
47. Liu, B.; Wang, Z.; Ghosh, S.; Zhou, Z. Defective ATM-Kap-1-mediated chromatin remodeling impairs DNA repair and accelerates senescence in progeria mouse model. *Aging Cell* **2013**, *12*, 316–318. [[CrossRef](#)]
48. Leon, K.E.; Buj, R.; Lesko, E.; Dahl, E.S.; Chen, C.W.; Tangudu, N.K.; Imamura-Kawasawa, Y.; Kossenkov, A.V.; Hobbs, R.P.; Aird, K.M. DOT1L modulates the senescence-associated secretory phenotype through epigenetic regulation of IL1A. *J. Cell. Biol.* **2021**, *220*, e202008101. [[CrossRef](#)]
49. Aird, K.M.; Worth, A.J.; Snyder, N.W.; Lee, J.V.; Sivanand, S.; Liu, Q.; Blair, I.A.; Wellen, K.E.; Zhang, R. ATM couples replication stress and metabolic reprogramming during cellular senescence. *Cell. Rep.* **2015**, *11*, 893–901. [[CrossRef](#)]
50. Yang, H.; Wang, H.; Ren, J.; Chen, Q.; Chen, Z.J. cGAS is essential for cellular senescence. *Proc. Natl. Acad. Sci. USA* **2017**, *114*, E4612–E4620. [[CrossRef](#)]
51. de Magalhães, J.P.; Chainiaux, F.; Remacle, J.; Toussaint, O. Stress-induced premature senescence in BJ and hTERT-BJ1 human foreskin fibroblasts. *FEBS Lett.* **2002**, *523*, 157–162. [[CrossRef](#)] [[PubMed](#)]
52. Gorbunova, V.; Seluanov, A.; Pereira-Smith, O.M. Expression of human telomerase (hTERT) does not prevent stress-induced senescence in normal human fibroblasts but protects the cells from stress-induced apoptosis and necrosis. *J. Biol. Chem.* **2002**, *277*, 38540–38549. [[CrossRef](#)] [[PubMed](#)]
53. Speck, S.H.; Ganem, D. Viral latency and its regulation: Lessons from the gamma-herpesviruses. *Cell. Host Microbe* **2010**, *8*, 100–115. [[CrossRef](#)] [[PubMed](#)]
54. Harms, P.W.; Harms, K.L.; Moore, P.S.; DeCaprio, J.A.; Nghiem, P.; Wong, M.K.K.; Brownell, I.; International Workshop on Merkel Cell Carcinoma Research (IWMCC) Working Group. The biology and treatment of Merkel cell carcinoma: Current understanding and research priorities. *Nat. Rev. Clin. Oncol.* **2018**, *15*, 763–776. [[CrossRef](#)]
55. Gelgor, A.; Gam Ze Letova, C.; Yegorov, Y.; Kalt, I.; Sarid, R. Nucleolar stress enhances lytic reactivation of the Kaposi’s sarcoma-associated herpesvirus. *Oncotarget* **2018**, *9*, 13822–13833. [[CrossRef](#)]
56. Nwogu, N.; Ortiz, L.E.; Kwun, H.J. Surface charge of Merkel cell polyomavirus small T antigen determines cell transformation through allosteric FBW7 WD40 domain targeting. *Oncogenesis* **2020**, *9*, 53. [[CrossRef](#)]
57. Alvarez Orellana, J.; Kwun, H.J.; Artusi, S.; Chang, Y.; Moore, P.S. Sirolimus and other mTOR inhibitors directly activate latent pathogenic human polyomavirus replication. *J. Infect. Dis.* **2020**, *224*, 1160–1169. [[CrossRef](#)]
58. Moore, P.S.; Chang, Y. Why do viruses cause cancer? Highlights of the first century of human tumour virology. *Nat. Rev. Cancer* **2010**, *10*, 878–889. [[CrossRef](#)]
59. Moens, U.; Macdonald, A. Effect of the Large and Small T-Antigens of Human Polyomaviruses on Signaling Pathways. *Int. J. Mol. Sci.* **2019**, *20*, 3914. [[CrossRef](#)]
60. Lill, C.; Schneider, S.; Item, C.B.; Loewe, R.; Houben, R.; Halbauer, D.; Heiduschka, G.; Brunner, M.; Thurnher, D. P53 mutation is a rare event in Merkel cell carcinoma of the head and neck. *Eur. Arch. Otorhinolaryngol.* **2011**, *268*, 1639–1646. [[CrossRef](#)]
61. Houben, R.; Dreher, C.; Angermeyer, S.; Borst, A.; Utikal, J.; Haferkamp, S.; Peitsch, W.K.; Schrama, D.; Hesbacher, S. Mechanisms of p53 restriction in Merkel cell carcinoma cells are independent of the Merkel cell polyoma virus T antigens. *J. Invest. Dermatol.* **2013**, *133*, 2453–2460. [[CrossRef](#)] [[PubMed](#)]
62. Bonifacio, L.N.; Jarstfer, M.B. MiRNA profile associated with replicative senescence, extended cell culture, and ectopic telomerase expression in human foreskin fibroblasts. *PLoS ONE* **2010**, *5*, e12519. [[CrossRef](#)] [[PubMed](#)]

63. Yosef, R.; Pilpel, N.; Papismadov, N.; Gal, H.; Ovadya, Y.; Vadai, E.; Miller, S.; Porat, Z.; Ben-Dor, S.; Krizhanovsky, V. p21 maintains senescent cell viability under persistent DNA damage response by restraining JNK and caspase signaling. *EMBO J.* **2017**, *36*, 2280–2295. [[CrossRef](#)] [[PubMed](#)]
64. Stein, G.H.; Dulić, V. Origins of G1 arrest in senescent human fibroblasts. *Bioessays* **1995**, *17*, 537–543. [[CrossRef](#)] [[PubMed](#)]
65. Prata, L.G.P.L.; Ovsyannikova, I.G.; Tchkonina, T.; Kirkland, J.L. Senescent cell clearance by the immune system: Emerging therapeutic opportunities. *Semin. Immunol.* **2018**, *40*, 101275. [[CrossRef](#)] [[PubMed](#)]
66. Verhaegen, M.E.; Mangelberger, D.; Weick, J.W.; Vozheiko, T.D.; Harms, P.W.; Nash, K.T.; Quintana, E.; Baciú, P.; Johnson, T.M.; Bichakjian, C.K.; et al. Merkel cell carcinoma dependence on bcl-2 family members for survival. *J. Invest. Dermatol.* **2014**, *134*, 2241–2250. [[CrossRef](#)] [[PubMed](#)]
67. Chteinberg, E.; Wetzels, S.; Gerritsen, W.; Temmerman, L.; van den Oord, J.; Biessen, E.; Kurz, A.K.; Winnepenninckx, V.; Zenke, M.; Speel, E.J.; et al. Navitoclax combined with Alpelisib effectively inhibits Merkel cell carcinoma cell growth. *Ther. Adv. Med. Oncol.* **2020**, *12*, 1758835920975621. [[CrossRef](#)]
68. Noren Hooten, N.; Evans, M.K. Techniques to Induce and Quantify Cellular Senescence. *J. Vis. Exp.* **2017**, *123*, e55533. [[CrossRef](#)]
69. Ge, S.X.; Son, E.W.; Yao, R. iDEP: An integrated web application for differential expression and pathway analysis of RNA-Seq data. *BMC Bioinform.* **2018**, *19*, 534. [[CrossRef](#)]
70. Feng, H.; Kwun, H.J.; Liu, X.; Gjoerup, O.; Stolz, D.B.; Chang, Y.; Moore, P.S. Cellular and viral factors regulating Merkel cell polyomavirus replication. *PLoS ONE* **2011**, *6*, e22468. [[CrossRef](#)]

Disclaimer/Publisher’s Note: The statements, opinions and data contained in all publications are solely those of the individual author(s) and contributor(s) and not of MDPI and/or the editor(s). MDPI and/or the editor(s) disclaim responsibility for any injury to people or property resulting from any ideas, methods, instructions or products referred to in the content.